THE EFFECT OF AGING ON THE MICROSTRUCTURE, PRECIPITATION RESPONSE, AND FATIGUE BEHAVIOR IN AN Al-Li-Cu ALLOY

J. F r a g o m e n i [1)], R. W h e e l e r [2)], K. V. J a t a [2)]

[1)]The University of Detroit Mercy
College of Engineering and Science
Department of Mechanical Engineering
Detroit, Michigan, USA

[2)]Air Force Research Laboratory
Metals, Ceramics and Nondestructive Evaluation Division
Materials and Manufacturing Directorate
AFRL/MLLMD, 2230 Tenth Street
Wright Patterson Air Force Base, Dayton, Ohio, USA

The interrelationships between precipitate characteristics and mechanical properties of an Al-Li-Cu alloy was quantified. The microstructure, precipitation response, and fatigue crack growth rates in the Al-Li-Cu alloy AF/C458 were studied following single and duplex aging treatments for varying aging times on specimens that were given a six percent stretch after solution heat treatment. Aging response was studied using hardness and compression yield strength measurements. Quantitative transmission electron microscopy methods were used to characterize average size, volume fraction, number density, and interparticle spacing of strengthening precipitates, δ' (Al$_3$Li) and T$_1$ (Al$_2$CuLi). Strength and fatigue crack growth rates for select heat treatments were obtained and were related to the precipitate microstructure and yield strength data.

Key words: Al-Li-Cu, aging, precipitation strengthening, quantitative microscopy, microstructure, fatigue, hardness, TEM.

1. INTRODUCTION

Aluminum-lithium alloys are being commercially used in military aircraft and space vehicles in various structural applications including the horizontal stabilizer, the lower wings, and upper wings. There is still, however, an interest in developing next generation aluminum-lithium alloys with improved specific strength and damage tolerance and reduced mechanical property anisotropy. Recently, the U.S. Air Force and Alcoa developed two aluminum-lithium-copper

alloys designated AF/C-489 and AF/C-458 [1–5] with 2.1 and 1.8 weight percent lithium, respectively. The AF/C-458 alloy has been shown to possess superior strength, damage tolerance properties [6] and stress corrosion cracking resistance [7, 8]. Studies by CSONTOS and STARKE recently [4, 5] compared precipitation and slip behavior between the AF/C-489 and AF/C-458 alloys by employing single aging and duplex aging. Duplex aging refers to where the alloy has been aged twice with two consecutive aging treatments and is sometimes referred to as "double aging". Single aging is where the alloy has been aged only once at one given aging treatment. CSONTOS and STARKE [4, 5] concluded that the lower ductility in AF/C-489 compared to AF/C-458 is due to a large grain size, a higher volume fraction of the $\delta\prime$ precipitates and enhanced planar slip and stress concentration at grain boundaries. Thus, AF/C-458 has been shown to have improved mechanical property benefits for aerospace structural applications as compared with other Li-containing aluminum base alloys [4]. In addition, the lower density of Al-Li-Cu C458 alloy (7.4% lower than 7050) should result in lower fuel consumption or increased payload in aircraft application.

The objective of this work was in part to understand the effect of artificial aging on the precipitate microstructure in the advanced aerospace Al-1.8wt%Li-2.7Cu-0.3Mg-0.5Zr-0.3Mn-0.8Zn alloy AF/C-458 and to study the effects of aging on Fatigue Crack Growth (FCG). The Air Force Research Laboratory and ALCOA developed the alloy AF/C-458 to achieve an elongation greater than 5% at the peak-strength condition. This alloy was a derivative of the previously developed Al-Li-Cu alloy AF/C-489 [9].

The precipitate characteristics are known [10–15, 22] to control the mechanical properties of age hardened aluminum alloys. In this research single and duplex aging studies were performed. In aluminum-lithium alloys, pre-age stretching prior to a duplex aging schedule has been found to greatly increase the ductility and fracture toughness [16–19]. Plastic deformation prior to aging has been found to enhance the precipitation response of Al-Li-Cu-X alloys AF/C 458 [4, 16, 17]. The increase in hardness and strength of the alloy by pre-stretching can be correlated to the microstructure precipitates [16]. Duplex aging is expected to enhance the matrix precipitation of the T_1 (Al$_2$CuLi) intermetallic strengthening phase leading to accelerated overaging. The presence of well-distributed T_1 precipitates was seen throughout the matrix and contributed to the strength and hardness of the alloy. Transmission electron microscopy was used to characterize average size, distribution, morphology, volume fraction, number density, and interparticle spacing of various intermetallic precipitates. The $\delta\prime$ and T_1 intermetallic precipitates were analyzed by quantitative microscopy methods for samples that had a six-percent deformation stretch and varying heat treating conditions.

2. Precipitation response

Microstructure of Al-Li alloy AF/C-458 was recently characterized by CSONTOS and STARKE [4]. The results of their studies show that precipitation in AF/C-458 is similar to that of other Al-Li-Cu alloys. Various precipitates encountered in this alloy are briefly described below.

The crystal structure of the T_1 (Al$_2$LiCu) phase is known to have an hexagonal crystalline structure. The T_1 phase was initially discovered by HARDY and SILCOCK [20] who determined its crystal structure as hexagonal with $a = 0.4965$ nm and $c = 0.9345$ nm. NOBLE and THOMPSON [21] observed the formation of plate-shaped precipitates on {111} planes in ternary Al-Li-Cu alloys comparable to ALCOA alloy 2090 and C458. NOBLE and THOMPSON [21] identified these plate shaped precipitates on {111} as the T_1 phase and also verified the orientation relationship originally proposed by HARDY and SILCOCK as {0001}$_{T1}$ //{111}$_{Al}$. The thin plates lie on {111} matrix planes, which means that three matrix slip planes intersect the plate at angles of 70.5° [19]. The T_1 particles provide a substantial strengthening [13] contribution to Al-Li-Cu alloys.

The precipitates are ordered, spherical, and coherent with the aluminum lattice and they also nucleate and coarsen/grow homogeneously in the matrix. The δ' (Al$_3$Li) phase has the ordered face-centered-cubic (fcc) or L1$_2$ (Cu$_3$Au) superlattice crystal structure and has a lattice parameter of a = 0.404+−0.003 nm [23, 25]. The cubic lattices of the δ' particles and the aluminum matrix are geometrically similar, having a small misfit strain on the order of −0.08+−0.02% [21, 26, 27]. The δ' (Al$_3$Li) phase orientation is the same as the fcc matrix that is {100}$_{\delta'}$ // {100}$_{Al}$.

Zirconium additions to aluminum-lithium alloys form the dispersoid β' (Al$_3$Zr) which substantially decreases the recrystallization of grains during ingot breakdown and hot rolling. The composite precipitates contain an inner core of Al$_3$Zr surrounded by an outer shell of the Al$_3$Li phase and resemble a ring-shaped or doughnut-shaped spherical type particles [28, 29].

The θ', (Al$_2$Cu), phase is not reported to be a stable phase in the C458 alloy. When formed in similar alloys, these precipitates lie on {001} habit planes. Their shape is that of very thin discs which are coherent with the aluminum matrix. This produces a strain field that contributes to the effectiveness of this precipitate as a strengthening dispersion in many Al-Cu base alloys. The coprecipitation of θ' with δ' has been observed in underaged alloys [28, 29].

3. Experimental methods

3.1. Hardness measurements

AF/C-458 plate Al-Li-Cu material was obtained from Alcoa in a $T3$ temper. The Al-Li-Cu alloy AF/458 was rolled at the Alcoa Davenport commercial rolling

mill. The plate had a six percent stretch after the solution heat treatment but prior to the aging treatment. Samples were machined directly from the Al-Li-Cu plate material and later artificially aged for both single and duplex aging practices. The heat treatments were carried out on one inch square coupons in ambient atmosphere under static air conditions. These coupons were quenched directly from the aging furnace into a water bath. A number of test coupons were aged at 150 C for various times and Rockwell B hardness measurements recorded. Hardness readings were made along the short transverse direction with parallel surfaces ground to a 600 grit finish. After determining the peak age condition for 150 C, a number of coupons were given duplex heat treatments consisting of the shortest time to achieve the peak age hardness at 150 C followed by various aging times at 190 C. Precipitation hardening due to aging was followed by hardness and compression yield strength measurements. The artificial aging response was determined based on hardness measurements. Artificial aging refers to aging done at some elevated temperature and is often just referred to as simply "aging".

3.2. TEM measurements

The average precipitate size, size distribution, number density, volume fraction, and interparticle spacing of the intermetallic strengthening precipitates δ' (Al_3Li) and T_1 (Al_2LiCu) were directly measured from TEM micrograph dark field images. The volume fractions of δ' (Al_3Li) and T_1 (Al_2LiCu) were also calculated based on the TEM foil thickness and average precipitates size. The TEM particle size measurements were done for all of the aging times and conditions for both the single aged conditions and the duplex/double aged conditions.

The TEM analysis was carried out on a Philips CM200 instrument equipped with a field emission source. Thin foil specimens were prepared by electropolishing 3 millimeter discs in a solution of 5% perchloric acid in methanol at a temperature of –40 C. Both the bright field and dark field images were recorded from each sample with the grain of interest oriented near <110> type crystallographic directions. Foil thickness required for the quantification of particle volume fractions and densities were measured using the fringe image of inclined T_1 particles belonging to other variants of this precipitate.

3.3. Particle size measurements

Particle size measurements were performed for both T_1 and Al_3Li precipitates directly from TEM images. Projected images of the actual particle sizes were measured. Based on standard quantitative microscopy theory and methods, the measurements of the projected images were converted to the actual real particle sizes. Two projected particle size diameter images were measured directly from the TEM micrographs for each particle. Thus an average size and aspect

ratio was determined for each individual particle of the entire distribution of particle sizes. For the nonspherical T_1 particles, size distribution histograms were determined from the size measurements. The average particle size was also determined based on the measurements of the projected particle images. The Al_3Li precipitates had a spherical shape morphology, and the T_1 particles had a disk shape particle morphology. The Al_3Li were a result of homogeneous nucleation within the microstructure, whereas the T_1 precipitates nucleated heterogeneously on dislocations within the microstructure.

4. RESULTS

4.1. Light microscopy, hardness and yield strength

The light microscopy microstructure of the alloy AF/C-458 in rolled plate form is shown in Fig. 1. This figure illustrates the conventional pancake shaped grains observed in aluminum-lithium alloy plate products. The aging response of the AF/C-458 plate, determined from hardness measurements, is given in Fig. 2. Open squares indicate the Rockwell B hardness of samples isothermally aged at 150 C as a function of time. The closed circles represent samples given an initial 24 hour heat treatment at 150 C followed by aging for additional times at 190 C. Here, times are given as a total of the 24 hour-150 C plus the time at 190 C. Data in Fig. 2 shows that even with duplex/double aging, hardness loss in AF/C-458 is minimal. Compressive buckling strengths obtained as a function of aging time are shown in this figure as well and are indicated by filled triangles.
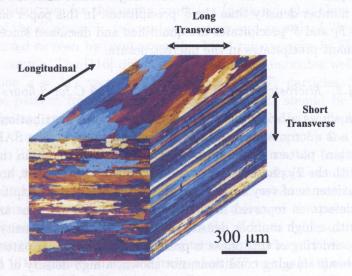

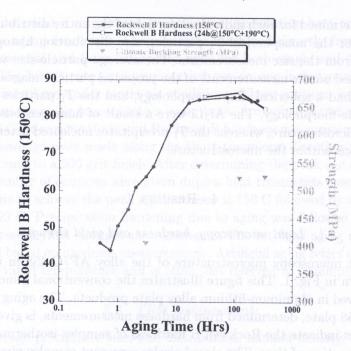FIG. 1. Light microscopy microstructure of 3/4 inch plate of the aluminum-lithium-copper alloy AF/C-458.

FIG. 2. Hardness of AF/C-458 as a function of single and duplex aging.

The precipitate phases that were observed included δ' (Al$_3$Li), T_1 (Al$_2$LiCu), β' (Al$_3$Zr), and θ' (Al$_2$Cu). For all of the aging times studied here, the composite Al$_3$Zr/Al$_3$Li particles were found to be much larger in size than the δ' but much fewer in the number density than the δ' precipitates. In this paper only observations on the T_1 and δ' precipitates are quantified and discussed since these were the predominant precipitates in the microstructure.

4.2. Microstructure of sample aged at 150 C for 3 hours

Figure 3a shows a bright field image of the uniform distribution of dislocations across a 2 micron square area of the microstructure. The SAD (Selected Area Diffraction) pattern in the insert of Fig. 3b does not contain the streaking associated with the T_1 phase. Some degree of diffusivity is present, however, suggesting the existence of very early stage nucleation events of precipitates related to the line defects as reported in the literature. The δ' particles are very fine in Fig. 3b with a high number density. Strong superlattice intensity consistent with the $L1_2$ ordering of this phase is present in the diffraction pattern. Finally, under weak beam imaging conditions, not shown, a high density of dislocations is evident but T_1 has not begun to nucleate. Higher magnification imaging would be required to resolve such events.
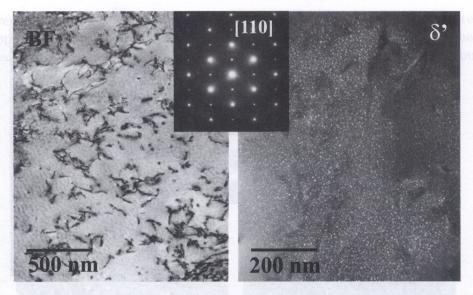
FIG. 3. TEM micrographs of the AF/C-458 sample aged for 3 hours at 150 C showing a) bright field image of dislocation segments and b) dark field image of δ' precipitates. Insert is a [110] diffraction pattern with {1100} superlattice intensity used to image the δ' particle.

4.3. Microstructure of samples aged at 150 C for 24 hours

The microstructure for this aging condition (peak aging) is shown in Fig. 4. Coarsening of the δ' phase, in (a), and nucleation and growth of T_1 particles, in (b), has occurred as seen by comparing the TEM micrographs in Fig. 3 for the 3 hour aged sample. The [110] diffraction pattern now indicates well-developed streaking along $g = 111$ vectors related to the thin T_1 particles. These were absent in the pattern from the 3 hour aged sample. It should be noted that each δ' precipitate now coexists with a very thin plate of the θ' phase within each particle. Since the habit plane for θ' precipitates is {001} and images are recorded near [110], only one variant of these discs is visible "edge-on". Close examination of the δ' particles in Fig. 4 indicates that about one third of these precipitates have the characteristic midline feature, oriented nearly along the vertical direction in the image. The other two thirds of the particles have a broad dark band oriented perpendicular to the θ' discs lying on (001). This image contrast results from the remaining two orientations of θ' discs. These lie on (100) and (010) planes which are inclined at 45° to the [110] electron beam direction. The thin "rib" of θ' within the δ' precipitates does not persist at the longer aging times discussed below.
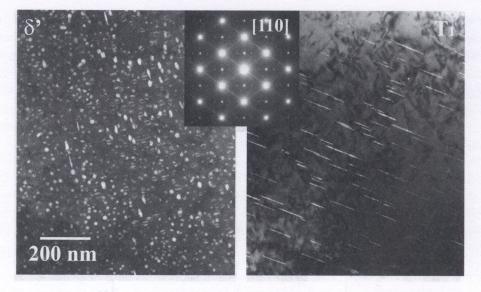
FIG. 4. Dark field TEM micrographs and the associated [110] diffraction pattern for the Al-Li-Cu AF/C 458 alloy aged at 150 C for 24 hours; a) δ' Al$_3$Li precipitates and b) T_1 Al$_2$LiCi precipitates.

4.4.   Microstructure of duplex aged samples

Long aging times at 150 C did not decrease the hardness, as illustrated in Fig. 2. Hence, a duplex aging treatment was implemented to promote overaging. This consisted of an initial aging of the samples at 150 C for 24 hours (peak age condition) followed by an additional treatment for various times at 190 C. Interestingly, from Fig. 2, these subsequent long aging times at 190 C caused little change in hardness once the peak age microstructure was established. Direct aging at 190 C has been reported to achieve significantly reduced strength and rapid overaging [4, 5]. Hence, the microstructures would be expected to coarsen and overaging to take place. Figure 5 shows the precipitate structure of the duplex aged sample given a secondary age for 96 hours at 190 C. Here, the δ' particles have coarsened and the θ' ribs within them have dissolved. For the T_1 particles, quantitative changes from the peak age microstructure are not so clear. Particle separation has also increased noticeably for the δ' precipitates and they are largely found in contact with T_1 plates. From Fig. 6, further aging at 190 C for 316 hours results in a microstructure composed entirely of δ' precipitates in contact with T_1 precipitates. While the size of the δ' particles is clearly greater than in the previous aging condition, any change in T_1 size is not obvious. The shape of the δ' precipitates is no longer spherical since they are growing in contact with the flat surfaces of the T_1 platelets. The morphologies of the two dispersed

strengthening phases are no longer simple and can not be considered discretely dispersed. The degree of the size changes is a key subject of this work where quantitative measurements of the strengthening particles have been carried out.
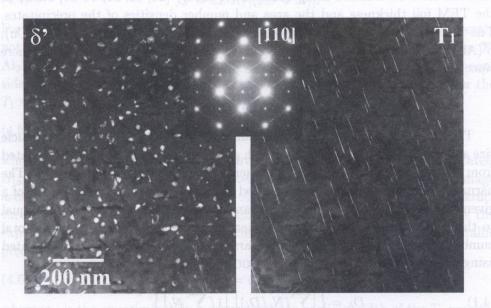

FIG. 5. TEM dark field images and the associated diffraction pattern showing coarsening of the a) δ' particles and b) T_1 precipitates after aging at 150 C for 24 hours followed by 190 C for 96 hours.

FIG. 6. TEM dark field images and the associated diffraction pattern showing coarsening of the a) δ' particles and b) T_1 precipitates after aging at 150 C for 24 hours followed by 190 C for 316 hours.
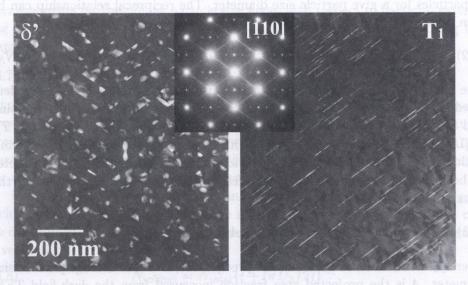
4.5. *Precipitates observed from TEM microscopy*

The experimentally measured planar particle sizes were converted into true particles sizes determined using quantitative theory [24, 30, 31, 34–36] based on the TEM foil thickness and the area and number densities of the precipitates. The precipitate phases that were observed included δ' (Al$_3$Li), T_1 (Al$_2$LiCu), β'(Al$_3$Zr), and θ' (Al$_2$Cu). Only δ' and T_1 particles have been quantified here since these are the dominant precipitate phases formed in this alloy.

4.6. *Quantitative microscopy measurements and analysis*

The harmonic diameters, equivalent diameters determined from both particle size and particle number density, for each given aging treatment will be tabulated from the planar particle size measurements of the δ' and T_1 precipitates. The harmonic diameters are can be correlated directly with average particle size of a given size distribution. The harmonic diameter is mathematically inversely equal to the sum of the reciprocals of the measured diameters divided by the total number of measured diameters. The harmonic diameters were thus calculated using the expression given by UNDERWOOD [30]

$$(4.1) \qquad D_h = \left\{ \left[\sum (N_i/D_i) \right] \left[1/\sum N_i \right] \right\}^{-1},$$

where D_h is the harmonic average particle size diameter, and N_i is the number of particles for a give particle size diameter. The reciprocal relationship can be seen more readily in the form [30]

$$(4.2) \quad 1/D_h = (N_1/D_1 + N_2/D_2 + \ldots + N_N/D_N)/(N_1 + N_2 + N_3 + \ldots + N_N)$$

The volume fraction of the precipitates in the microstructure were also calculated from the experimental data. For the Al$_3$Li precipitates both overlapping and truncation effects were incorporated into the calculations. However for T_1, Al$_2$LiCu, only the truncation effect was included in the volume fraction determinations since the overlapping was not evident. For spherical particles of diameter D both overlapping and truncation effects were taken into account using the equation given by [30]

$$(4.3) \qquad f_{\delta'} = [-2\ln(1 - A)][D/(D + 3t)],$$

where $f_{\delta'}$ is the volume fraction of δ' precipitates, D is the average particle size diameter, A is the projected area fraction measured from the dark-field TEM micrographs, and t is the TEM foil thickness. For the situation where there are very large spherical particles with very overaged alloys, the effect of particle

overlapping is small, but the effect of truncation at the foil surface needs to be considered. Thus for foil truncation effect only the above equation becomes [30]

$$(4.4) \qquad f_{\delta'} = 2DA/[(2D + 3t)].$$

For the T_1 precipitates the particle overlapping is very small and subsequently not important so only the truncation effects need to be considered. The T_1 Al$_2$LiCu intermetallic precipitates are disk shaped (not spherical) so thus considering the measured planar length of the T_1 precipitates, the expression for the T_1 volume fraction, f_{T1}, can be written as

$$(4.5) \qquad f_{T1} = (4A_{pl}N_{total})[2l_{pl}/(2l_{pl} + 3t)]/A_{total},$$

where l_{pl} is the experimentally measured planar length of the T_1 precipitates, N_{total} is the total number of precipitates on the measured plane of TEM image area, t is the TEM foil thickness, and A_{total} is the total area of the microstructure field of view from which the particles are being measured, and A_{pl} is the experimentally measured planar particle area. For the T_1 Al$_2$LiCu intermetallic precipitates, A_{pl} can be expressed as

$$(4.6) \qquad A_{pl} = l_{pl}w_{pl},$$

where w_{pl} is the experimentally measured planar particle width of the T_1 precipitates and l_{pl} is the experimentally measured planar length of the T_1 precipitates.

The edge effect were also taken into account when doing the particle size measurements for the planar particle size areas with respect to particles extending beyond the field of view. The edge effects were incorporated by using the expression [30]

$$(4.7) \qquad N_{total} = \{N'' + (N'/2)\}/A_{total},$$

where N' is the number of particles intersected by the edges of the field of the microstructure, N'' is the number of particles lying in field of view microstructural area, A_{total} is the total area of the microstructure field of view from which the particles are being measure, and N_{total} is the total number of particles corrected for edge effect within the microstructural area image field of view.

Based on the harmonic diameters and the foil thickness, the number of particles per unit volume i.e., the volume number density, of the precipitates can be determined. The volume number density can be determined from the formula given by [31]

$$(4.8) \qquad N_{volume} = N_{total}\{t + (\pi D_h/2)\}^{-1},$$

where N_{volume} is the total number of intermetallic precipitate particle per unit volume, i.e the volume number density, and t is the thin foil thickness. Thus,

based on the volume number density of precipitates, the true particle size diameter can be predicted from the equation given by [31]

$$(4.9) \qquad D_{\text{true}} = \{N_{\text{total}}/N_{\text{volume}}\} - t.$$

Here D_{true} is the actual true average particle size diameter for the distribution of intermetallic precipitate particles within the microstructure. For very small thin foil, the true particle size diameter can be estimated by the equation given by

$$(4.10) \qquad D_{\text{true}} = \{N_{\text{total}}/N_{\text{volume}}\} = \{\pi/2\}D_h,$$

where D_h is the harmonic average particle size diameter.

The harmonic diameter [30], is used to convert the experimentally measured planar particle sizes to the actual true particle sizes. Thus, the harmonic diameter is very important for determining the true average particle size of a distribution of particle sizes.

4.7. Quantitative TEM microscopy

Tables 1–4 summarize the experimental quantitative measurements and the calculated microstructure parameters for the Al-Li-Cu AF/C458 alloy. Tables 1 and 2 show the data for δ' precipitates and Tables 3 and 4 show the data for T_1. The general trend given the limited aging data shown in Fig. 7 is for δ' volume fraction to decrease while T_1 volume fraction increases with aging time. This is consistent with a depletion of Li from the δ' phase in order to accommodate the growth of T_1. The extent of this transfer of Li would then be limited by Cu availability. Only after all excess Cu has been depleted from the non-equilibrium θ' phase and from the matrix, will the volume fraction of the two phases reach equilibrium. (This is because at 24 hours, θ' is seen as midrib of δ' precipitates.)

In Fig. 8, the number density of T_1 decreases slowly from a peak value near 24 hours aging time. This indicates great thermodynamic stability of the T_1

Table 1. **Experimentally measured quantitative microstructure particle size data for δ'-Al$_3$Li intermetallic precipitates for both single and duplex aged AF/C-458 Al-Li-Cu alloy samples, prestretch six percent prior to aging.**

Aging temps. (C)	Aging times (hrs)	r_{planar} (nm)	No of particles measured	Average aspect ratio	Spherical morphology (%)	TEM foil thickness (nm)	Harmonic diameter (nm)
150	3	4.05	18	0.7781	45.5	20	4.14
150	24	8.25	34	0.7198	42.94	22	10.2
150 & 190 (duplex aged)	24 & 96 (duplex aged)	7.81	34	0.7174	42.19	11	15.3
150 & 190 (duplex aged)	24 & 316 (duplex aged)	12.85	242	–	–	25	18.8

Table 2. Calculated quantitative microstructure particle size data for δ'-Al_3Li intermetallic precipitates for both single and duplex aged AF/C-458 Al-Li-Cu samples, prestretch six percent prior to aging.

Aging temps. (c)	Aging times (hours)	Area density number (nm)$^{-2}$ N_A	Volume number density (nm)$^{-3}$ N_v	TEM foil thickness (nm)	Volume fraction with both overlapping & truncation effects	True average particle size diameter D_{true} (nm)	Average inter-particle spacing distance (nm)
150	3	11.75E(-3)	4.43E(-4)	20	0.02433	6.5	22.407734
150	24	19.02E(-4)	5.00E(-5)	22	0.09121	16.02	35.734216
150 & 190 (duplex aged)	24 & 96 (duplex aged)	3.8E(-4)	1.09E(-5)	11	0.04698	24.03	87.555069
150 & 190 (duplex aged)	24 & 316 (duplex aged)	3.1E(-4)	5.61E(-5)	25	0.09121	29.53	113.8

Table 3. Experimentally measured quantitative microstructure particle size data for T_1-Al_2LiCu intermetallic precipitates for both single and duplex aged AF/C-458 Al-Li-Cu alloy samples, prestretch six percent prior to aging.

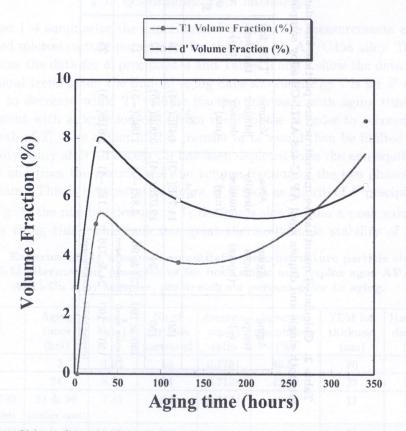| Aging temp (C)	Aging time (hrs)	l_{planar} (nm)	Width (nm)	No. of particles measured	TEM foil thickness (nm)	Harmonic length (nm)	Standard deviation of l_{planar} (nm)
150	24	68.515	4.255	163	22	35.4	33.639135
150 & 190 (duplex aged)	24 & 96 (duplex aged)	61.41	4.16	117	11	32.8	26.946992
150 & 190 (duplex aged)	24 & 316 (duplex aged)	75.4	6.25	294	25	43.5	38.892341
150 & 190 (duplex aged)	24 & 316 (duplex aged)	89.418	6.25	310	25	45.2	41.480962

FIG. 7. Volume fraction of the T_1 Al_2LiCu precipitates and the Al_3Li precipitates as a function of single and duplex aging treatments of the Al-Li-Cu Alloy AF/C458.

Table 4. Calculated quantitative microstructure particle size data for T_1–Al_2LiCu intermetallic precipitates for both single and duplex aged AF/C-458 Al-Li-Cu alloy samples, prestretch six percent prior to aging.

Aging temp (C)	Aging time (hrs)	Area number density (nm)$^{-2}$	Volume number density (nm)$^{-3}$	TEM foil thickness (nm)	True average particle size diameter D_{true} (nm)	Volume fraction without truncation effect	Volume fraction with truncation effect
150 (duplex aged)	24 (duplex aged)	6.87E(-4)	8.85E(-5)	22	55.6	0.2714882	0.0749123
150 & 190 (duplex aged)	24 & 96 (duplex aged)	4.89E(-4)	7.81E(-5)	11	51.5	0.4833953	0.0868984
150 & 190 (duplex aged)	24 & 316 (duplex aged)	6.38E(-4)	6.84E(-4)	25	68.3	0.678923	0.0705671
150 & 190 (duplex aged)	24 & 316 (duplex aged)	7.14E(-4)	7.446E(-4)	25	71.0	0.784321	0.0765891

phase once sufficient particle size is achieved. Specifically, this size results in a continuous skeleton of interconnected T_1 platelets. The connectivity of the T_1 particles can be deduced from the observation that the particle size and center-to-center spacing, shown in Figs. 9 and 10, respectively, are equal (each
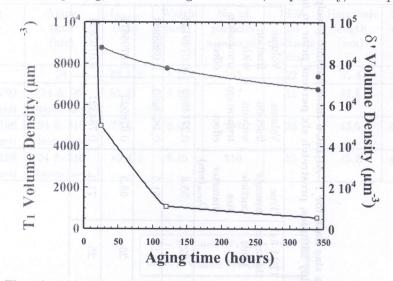

FIG. 8. The volume densities of the T_1 Al$_2$LiCu precipitates and the Al$_3$Li precipitates as a function of single and duplex aging conditions of the Al-Li-Cu Alloy AF/C458.
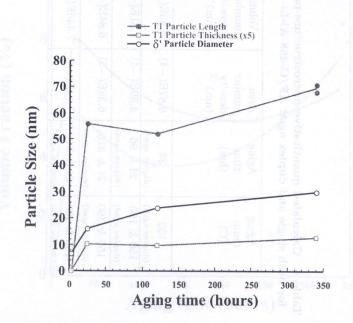

FIG. 9. Particle size results for the T_1 Al$_2$LiCu precipitates and the Al$_3$Li precipitates as a function of single and duplex aging conditions of the Al-Li-Cu Alloy AF/C458.
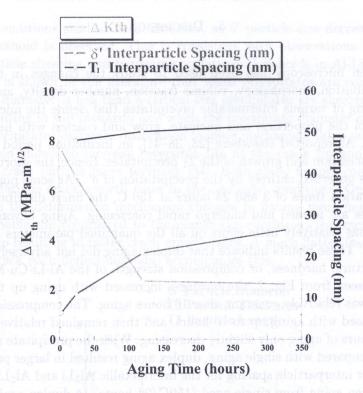
FIG. 10. Fatigue threshold and precipitate interparticle spacing of Al-Li-Cu AF/C458 as a function of aging time, (b) fatigue threshold as a function of interparticle spacing and (c) fatigue threshold as a function of precipitate diameter.

approximately 50 nm). In contrast, the δ' size changes rapidly while precipitates remain relatively discrete (i.e. for aging times less than 96 hours of the duplex heat treatment). At later times, contact made with T_1 particles may contribute to slower rates of charge.

4.8. Fatigue crack growth rates

FCG rates for the single and duplex aging treatments were obtained for $R = 0.1$ at 30 Hz in laboratory air. Standard ASTM fatigue crack growth specimens were machined directly from the Al-Li-Cu rolled alloy plate material. As illustrated by Fig. 10, the FCG results shows that the underaged alloy has the best FCG resistance and the longest overaged condition shows the least FCG resistance.

5. DISCUSSION

Electron microscopy has been used to study the changes in the average size, distribution, morphology, volume fraction, number density, and interparticle spacing of various intermetallic precipitates that define the microstructure and control the properties, and nucleate, grow and coarsen with heat treating and aging. As reported elsewhere [23, 38–41], an incubation period is required prior to nucleation and growth of the T_1 precipitates. Hence, the short time aging response is governed entirely by the precipitation of δ'. At some point between the observation times of 3 and 24 hours at 150 C, the finest distributions of T_1 precipitates are formed and undergo rapid coarsening. Aging beyond 24 hours at 190 C has relatively little effort on all the quantified parameters reported in Figs. 6–10. These results indicate that duplex aging did not adversely affect the microstructure, hardness, or compression strength of the Al-Li-Cu-Mg-Zr alloy C458. As seen from Fig. 2, the hardness increased with aging up to 10 hours and then was relatively constant after 10 hours aging. The compression strength also increased with aging up to 10 hours, and then remained relatively constant after 10 hours of aging only slightly decreasing. With the precipitate microstructure, as compared with single aging, duplex aging resulted in larger particle sizes and greater interparticle spacing for the intermetallic Al_3Li and Al_2LiCu precipitates. When going from single aged (150C/24 hours) to duplex aged (150C/24 hours and 190C/96 hours) the particle size increased by about 50% and the interparticle spacing was about 2.5 larger for the intermetallic Al_3Li precipitates. Further increasing the duplex aging to (150C/24 hours and 190C/316 hours) resulted in an greater increase in both size and spacing (see Table 4). However, with the T_1 (Al_2LiCu) precipitates, much smaller increases were seen with the size of T_1 as a consequence of the duplex aging (see Table 4 and Fig. 8). For the Al_3Li precipitates, both the particle overlapping and particle truncation effects were incorporated in the quantitative analysis. However, with the Al_2LiCu precipitates, only truncation effects were included in the analysis since particle overlapping was not seen with T_1. As compared with single aging, the volume number densities of both the T_1 and Al_3Li was seen to decrease as a consequence of the duplex aging (see Table 4 and Fig. 8). As seen from Fig. 8, there was a greater decrease in the volume number densities of Al_3Li than with the T_1 particles with aging.

Fatigue thresholds observed in this Al-Li alloy system are shown, together with the interparticle spacing, as a function of aging time in Fig. 10. The dependence of fatigue thresholds for various aging treatments are also shown as a function of particle size in Fig. 11. These graphs show that most significant variation in FCG thresholds is observed for δ' particle size. Neither the T_1 particle size nor the spacing appears to significantly affect the fatigue threshold for

the aging conditions studied here. However, as δ' particle size decreases higher fatigue threshold is observed. This is consistent with observations on the effects of particle shearing and bypassing on fatigue thresholds in Al-Li-Cu alloys [32, 33]. It is shown in the literature that when precipitates are coherent and precipitate diameter is less than a critical-size precipitates are sheared by dislocations resulting in slip planarity and when the precipitate diameter exceeds the critical (precipitate) diameter dislocation looping mechanism takes over. Planar slip has been shown to increase reversible slip at the crack tip and crack deflection or crack path is more tortuous [34]. Both these factors contribute to the slower fatigue crack growth rates in the less aged conditions. On the other hand, when the deformation mechanism changes to having more homogeneous slip, irreversible slip (compared to the planar slip condition) is accumulated at the crack tip resulting in faster crack growth rates. A much flatter fracture path (or lower crack path deflections) also accompanies this.
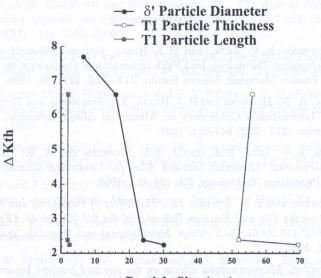

FIG. 11. The relationship between particle diameter and fatigue crack threshold for the four aged Al-Li-Cu AF/C458 samples.

6. CONCLUSIONS

The microstructural features of an Al-Li-Cu alloy C458 were characterized to determine the average size, distribution, number density, spacing, and volume fraction of the intermetallic strengthening precipitates Al_3Li (δ') and Al_2LiCu (T_1). Four aging treatments were used to quantify microstructure and precipitate

characteristics to the fatigue crack growth thresholds for the alloy AF/C-458. As aging progressed interparticle spacing between δ' particles and precipitate diameter increased more strongly than the T_1. FCG results on AF/C-458 are consistent with the observation of the fatigue threshold being higher for conditions of planar slip. The present aging conditions used here suggest that δ' particles may have a stronger effect than the T_1 precipitates. However, work is being carried out to validate these results to a much broader aging condition window.

ACKNOWLEDGMENTS

REFERENCES

1. A. K. HOPKINS, K.V. JATA, and R.J. RIOJA, *Isotropic Wrought Aluminum-Lithium Plate Development Technology*, [in:] Fifth International Conference on Aluminum Alloys, Grenoble, France, Materials Science Forum, **217–222**, 421–426, 1996.

2. K.V. JATA, A. K. HOPKINS and R.J. RIOJA, *The Anisotropy and Texture of Al-Li Alloys* [in:] Fifth International Conference on Aluminum Alloys, Grenoble, France, Materials Science Forum, **217–222**, 647-652, 1996.

3. V.K. JAIN, K.V. JATA, R.J. RIOJA, J.T. MORGAN and A. K. HOPKINS, *Processing of an Experimental Aluminum-Lithium Alloy for Controlled Microstructure*, Journal of Materials Processing Technology, **73**, 108–118, 1998.

4. A.A. CSONTOS and E.A. STARKE JR., *The Effect of Processing and Microstructure Development on the Slip and Fracture Behavior of the 2.1 Wt Pct Li AF/C-489 and 1.8 Wt Pct Li AF/C-458 Al-Li-Cu-X Alloys*, Metallurgical and Materials Transactions A, **31A**, 1965–1976, 2000.

5. A.A. CSONTOS, *Microstructural effects on the slip and fracture behavior of isotropic Al-Li-Cu-X alloys*, Ph.D. Thesis, 1–205, University of Virginia, 2001.

6. Aluminum-Lithium Alloys, Bass-Lake Workshop Report, August 18, 1998, Bass Lake Lodge, Wright-Patterson Air Force Base, Ohio, organized/edited by K.V. Jata, Materials Directorate, WPAFB, 1–238, 1998.

7. D. MATHUR, *Localized corrosion and stress corrosion cracking studies of Al-Li-Cu alloy AF/C-458*, M.S. Thesis, Ohio State University, 1–190, 2000.

8. J.E. KERTZ, P.I. GOUMA and R.G. BUCHHEIT, *Localized Corrosion Susceptibility of Al-Li-Cu-Mg-Zn Alloy AF/C458 due to Interrupted Quenching from Solutionizing Temperatures*, Metallurgical and Materials Transactions A., **32A**, **10**, 2561-2573A, 2001.

9. V.K. JAIN, K.V. JATA, R.J. RIOJA, J.T. MORGAN and A.K. HOPKINS, *Processing of an Experimental Aluminum-Lithium Alloy for Controlled Microstructure*, Journal of Materials Processing Technology, **73**, 108–118, 1998.

10. W. CASSADA, *Heterogeneous Precipitation in Al-Li-Cu Alloys*, Ph.D. Thesis, University of Virginia, 1–187, 1987.

11. C.P. BLANKENSHIP, *Optimizing Mechanical Properties in Al-Li-X Alloys by Microstructural Design*, Ph.D. Thesis, University of Virginia, 4–129, 1992.

12. M. TAMURA, T. MORI and T. NAKAMURA, *Precipitation of Al_3Li from an Al-3.0wt.%Li Alloy and Some Properties of Al_3Li*, Journal Japanese Institute of Metals, **34**, 919–925, 1970.

13. J.C. HUANG, and A.J. ARDELL, *Precipitation of Al_3Li from an Al-3.0wt.%Li Alloy and Some Properties of Al_3Li*, Journal De Physique, **48**, C3, 373–383, September 1987.

14. C.P. BLANKENSHIP JR. and E.A. STARKE JR., *Mechanical Behavior of Double-Aged AA8090*, Metallurgical Transactions A, **24A**, 833–841, 1993.

15. J.F. NIE, B.C. MUDDLE, and I.J. POLMEAR, *The Effect of Precipitate Shape and Orientation on Dispersion Strengthening in High Strength Aluminum Alloys*, Material Science Forum, **217–222**, 1257–1262, 1996.

16. B.M. GABLE, A.A. CSONTOS, and E.A. STARKE, JR., *The Role of Mechanical Stretch on the Processing-Microstructure-Property Relationships of AF/C 458*, Materials Science Forum, **331–337**, 1341–1346, 2000.

17. W.A. CASSADA, G.J. SHIFLET and E.A. STARKE, JR., *The Effect of Plastic Deformation on T_1 Precipitation*, Journal De Physique, **48**, C3, 397–406, September 1987.

18. C.P. BLANKENSHIP JR., E. HORNBOGEN and E.A. STARKE JR., *Predicting Slip Behavior in Alloys Containing Shearable and Strong Particles*, Materials Science and Engineering, **A169**, 33–41, 1993.

19. C.P. BLANKENSHIP JR, and E.A. STARKE JR, *Structure-Property Relationships in Al-Li-Cu-Mg-Ag-Zr Alloy X2095*, Acta Metallurgical Materialia, **42**, 3, 845–855, 1994.

20. H.K. HARDY and J.M. SILCOCK *The Phase Sections at 500 C and 350 C of Aluminum-Rich Aluminum-Copper-Lithium Alloys*, Journal Institute of Metals, **84**, 423, 1955–1956.

21. B. NOBLE and G.E. THOMPSON, *Precipitation Characteristics of Aluminum-Lithium Alloys*, Metal Science Journal, **5**, 357–364, 1971.

22. Z.X. LI, R.A. MIRSHAMS, E.A. KENIK and P.J. HARTLEY, *Effect of Stretch Prior to Aging on Mechanical Properties in Al-Cu-Li, 2195, Alloy*, Light Weight Alloys for Aerospace Applications IV, E.W. LEE, W.E. FRAZIER, N.J. KIM, and K. JATA [Eds.], The Minerals, Metals and Materials Society, 117–127, 1997.

23. J.M. SILCOCK, *The Structural Aging Characteristics of Aluminum-Lithium-Copper Alloys*, Journal Institute of Metals, **88**, 357–364, 1959–60.

24. M.F. ASHBY and R. EBELING, *On the Determination of the Number, Size, Spacing, and Volume Fraction of Spherical Second-Phase Particles from Extraction Replicas*, Transactions of the Metallurgical Society of AIME, **236**, 1396–1404, 1966.

25. W.D. JONES and P.P. DAS *The Solubility of Li in Al*, Journal Institute of Metals, **87**, 338–340, 1959.

26. D.B. WILLIAMS and J.W. EDINGTON, *The Precipitation of $\delta'(Al_3Li)$ in Dilute Aluminum-Lithium Alloys*, Metal Science Journal, **9**, 529–532, 1975.

27. S.F. BAUMANN and D.B. WILLIAMS, *A New Method for the determination of the Precipitate-Matrix Interfacial Energy*, Scripta Metallurgica, **18**, 611–618, 1984.

28. P.L. MAKIN and B. RALPH *On the Aging of Aluminum-Lithium-Zirconium Alloy*, Journal of Materials Science, **19**, 3835–3843, 1984.

29. F.W. GAYLE and J.B. VANDER SANDE, *Composite Precipitates in an Al-Li-Zr Alloy*, Scripta Metallurgica, **18**, 473–478, 1984.

30. E.E. UNDERWOOD *Quantitative Stereology*, Addison-Wesley Publishing Company, Reading, Massachusetts, 1–175, 1970.

31. J.E. HILLIARD, *The Counting and Sizing of Particles in Transmission Microscopy*, Transactions of the Metallurgical Society of AIME, **224**, 906–917, 1962.

32. E. HORNBOGEN and K.-H. ZUM GAHR, *Microstructure and Fatigue Crack Growth in a γ- Fe-Ni-Al Alloy*, Acta Metallurgica, **24**, 581–592, 1976.

33. K.V. JATA and E.A. STARKE, *Fatigue Crack Growth and Fracture Toughness Behavior of an Al-Li-Cu Alloy*, Metallurgical Transactions, **17A**, 1011–1026, 1986.

34. A.K. VASUDEVAN, K. SADANANDA, *Classification of Fatigue Crack Growth Behavior*, Metallurgical and Materials Transactions, **26A**, 5, 1221–1234, 1995.

35. C.W. CORTI, P. COTTERILL and G.A. FITZPATRICK, *The Evaluation of the Interparticle Spacing in Dispersion Alloys*, International Metallurgical Reviews, The Metals Society, **19**, 77–88, 1974.

36. P.L. GOLDSMITH, *The Calculation of True Particle Size Distributions From the Size Observed in a Thin Slice*, British Journal of Applied Physics, **18**, 81-3-830, 1967.

37. J.M.G. CROMPTON, R.M. WAGNHORNE and G.B.BROOK, *The Estimation of Size Distribution and Density Precipitates From Electron Micrographs of Thin Foils*, British Journal of Applied Physics, **17**, 1301–1305, 1966.

38. D.B. WILLIAMS and J.W. EDINGTON, *The Precipitation δ′ (Al₃Li) of in Dilute Aluminum-Lithium Alloys*, Metal Science, **9**, 529–532, 1975.

39. G. THOMAS and J. NUTTING, *The Ageing Characteristics of Aluminum Alloys*, Journal of the Institute of Metals, **88**, 81–90, 1959–60.

40. P.L. MAKIN, and B. RALPH, *On the Ageing of an Aluminum-Lithum-Zirconium Alloy*, Journal of Material Science, **19**, 3835–3843, 1984.

41. L. CHEN, and Y. WANG, *The Continuum Field Approach to Modeling Microstructural Evolution*, Journal of Metals, **48**, 12 12–18, 1996.